Draft version April 13, 2023
Typeset using LaTeX **twocolumn** style in AASTeX631

Searching for and placing limits on the γ-ray emission from CHIME/FRBs using *Swift*/BAT GUANO data

Maxwell A. Fine[1]

[1] *University of Toronto*
Student Number: 1004714400

ABSTRACT

Fast radio bursts (FRBs) are brief radio pulses with unknown extragalactic origins. So far FRBs have only been detected at radio frequencies. Several FRB progenitor models propose that these bursts originate from magnetars, and predict associated γ-ray emission. Previous γ-ray searches have only examined two repeating FRB sources. This study used data from the *Swift*/BAT telescope which was obtained with GUANO to analyze 380 CHIME/FRB targets. I made an analysis pipeline that estimates the peak Signal-To-Noise Ratio (S/N) for each target, and determines fluence limits. I used seven energy bands ranging from 10-350 keV for S/N and 10-150 keV for fluence, 13 timescales from 0.01 to 6 seconds and 6 spectrum models. I used a search window of 6 s around the FRB observation in radio wavelengths. S/N estimates were determined for 244 sources analyzed, no FRBs were detected. Fluence limits were determined for 49 FRBs at a level of $\sim 10^{-7}$ ergs cm^{-2} in the 10-150 keV band (95% confidence). It is possible that nearby FRBs could be detected by *Swift*/BAT, and future research will focus on addressing issues that led to failures in the analysis of targets and analyzing a larger CHIME/FRB catalog.

1. INTRODUCTION

Fast radio bursts (FRBs) are short-duration broadband radio pulses of unknown extragalactic origin. The burst duration of FRBs in radio bands is milliseconds long, with peak flux densities of $\sim 0.1 - 10$ Jy at ~ 1 GHz (Petroff et al. 2022). FRBs were first discovered in 2007 (Lorimer et al. 2007).

FRBs have thus far only been observed at radio frequencies, specifically from 110 MHz to 8 GHz (Chawla et al. 2020; Gajjar et al. 2018; Pleunis et al. 2021).

Fast Radio Bursts (FRBs) are characterized by a phenomenon known as Dispersion Measure (DM), which causes a frequency-dependent arrival time delay. The DMs of FRBs have been measured to exceed the expected DM from sources within the Milky Way, strongly suggesting that FRBs originate from beyond our galaxy (Petroff et al. 2022). The number of published FRBs has now surpassed 800 sources, with 28 of them being repeaters[1], and 19 host galaxies have been identified (Petroff et al. 2022).

Corresponding author: Maxwell A. Fine
maxwell.fine@mail.utoronto.ca

[1] FRB catalog: https://www.herta-experiment.org/frbstats/

The driving mechanism(s) behind the bursts remains mysterious (Petroff et al. 2022; Platts et al. 2019). There are several proposed models, most of which involve magnetars. The magnetar based models can be put into two broad categories, a "shock-wave" and a "magnetosphere". For both models, emission is expected to happen close temporally to the radio emission and have similar burst duration. However, other models predict delayed emission or continuous emission of the γ-ray counterpart.

In the "shock-wave" model, synchrotron maser emission at ultrarelativistic magnetized shocks produces the FRB (Wu et al. 2020). In the magnetosphere model, reconnection of the magnetar's magnetic field drives emission (Lu et al. 2020). The main observational difference between the two models is at what distance from the magnetar emission is generated. For the shock-wave model, emission is generated $\gtrsim 10^5$km, and for the magnetosphere model, it is $\lesssim 10^5$km. So far observations have not been able to distinguish between the two models as finer time resolution observations are required to distinguish between the two models (Petroff et al. 2022).

Of particular interest is the burst from SGR-1935 + 2154, on April 28, 2020. SGR-1935 + 2154 is a magnetar within our own galaxy, which was first discovered in 2014 by the *Swift* telescope. The burst that occurred

in 2020 was a mega-Jansky burst that was detected by both STARE2 and CHIME/FRB. This radio burst was found to have a hard X-ray counterpart (Mereghetti et al. 2020; Bochenek et al. 2020; CHIME/FRB Collaboration et al. 2020), which provides a link between FRBs and magnetars. While this event was 30 times less luminous than the least-luminous extragalactic FRB, it is considered an 'FRB-like' burst due to the fact that CHIME/FRB would have classified it as an FRB if it had been detected outside of our galaxy (Petroff et al. 2022). The burst from SGR1935+2154 may represent the lower end of the luminosity range for FRBs (Bochenek et al. 2020; Petroff et al. 2022; CHIME/FRB Collaboration et al. 2020).

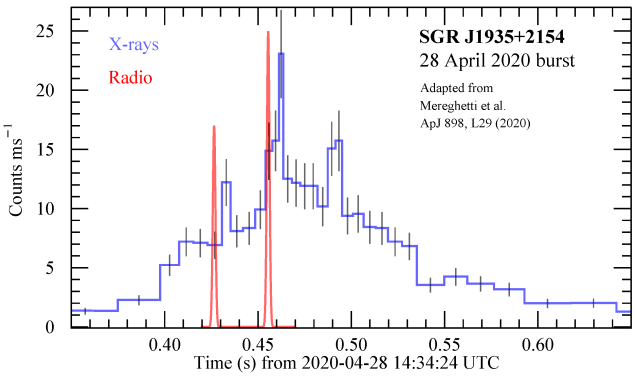

Figure 1: The time profile of the bright X-ray burst with energy range 20-200 keV emitted by Soft Gamma Repeater (SGR) J1935, which is associated with FRB 20200428A, was obtained using INTEGRAL/IBIS-ISGRI. In comparison, the radio pulses of FRB 20200428A as observed with CHIME are shown in the red profile. Figure from Petroff et al. (2022).

Despite predictions for γ-ray counterparts, FRBs have only been detected in radio wavelengths. There have been recent searches for associated γ-ray emission from FRBs (Scholz et al. 2017, 2020; Nicastro et al. 2021). Those searches were constrained to 2 repeating FRB targets. They made no detections but were able to establish fluence limits of $\sim 10^{-7}$ ergcm^{-2} in the 8 - 1000 keV band (Martone et al. 2019). One of the primary limitations of those searches was having simultaneous radio and X-ray & γ-ray observations of the FRB due to FRB's short duration. To guarantee simultaneous observations previous γ-ray searches choose to observe known repeating FRBs (Nicastro et al. 2021).

1.1. Swift/*BAT & CHIME/FRB*

Here I used the *Swift*'s Burst Alert Telescope (*Swift*/BAT) shown in fig 3 search for and place limits on γ-ray counterparts to FRBs. The primary benefit of using *Swift*/BAT for the search over more sensitive telescopes is the comparatively large number of FRB datasets available. *Swift*/BAT has data corresponding to over 500 Canadian Hydrogen Intensity Mapping Experiment (CHIME) FRB detections. The *Swift*/BAT data for the FRBs has been data collected using Gamma-Ray Urgent Archiver for Novel Opportunities (GUANO).

The *Swift* observatory was launched in 2004. *Swift* has three telescopes, one of which is the Burst Alert Telescope (BAT) which is a γ-ray telescope. BAT does not detect γ-rays directly, but rather detects the shadow cast by them using a pixelated lead mask. BAT has a detection energy range of 15-150 keV for imaging, and up to 350 keV for non-imaging. BAT looks at $\sim \frac{1}{8}$ the sky at any given time (Gehrels et al. 2004; Barthelmy et al. 2005).

The CHIME (shown in fig 2) radio telescope has a remarkable ability to detect FRBs owing to its wide field-of-view spanning approximately 200 square degrees, and frequency coverage of 400-800 MHz. CHIME has detected over 800 FRBs (Bandura et al. 2014; Petroff et al. 2022).

Figure 2: Photograph of the Canadian Hydrogen Intensity Mapping Experiment (CHIME) radio telescope in British Colombia Canada. CHIME is a radio interferometer. Image credit CHIME collaboration.

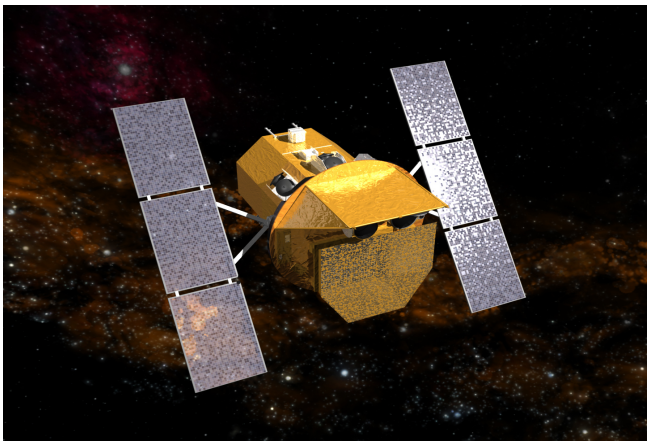

Figure 3: Artist impression of the *Swift* observatory in space. Image credit NASA.

GUANO has data corresponding to over 500 FRB events. GUANO has been running since January 2020 (Tohuvavohu et al. 2020). Prior to GUANO, the *Swift*/BAT telescope due to limited telemetry only sent data to Earth when it's onboard computer determined there was a γ-ray Burst (GRB) or other detection [2]. Unless sent to Earth, the data would then be over-written with the next observation and lost. GUANO added the ability to archive *Swift*/BAT data whenever there is a trigger sent from the ground (Tohuvavohu et al. 2020). In our case, the triggers are from CHIME/FRB when they detect a FRB. (CHIME Collaboration et al. 2022; Tohuvavohu et al. 2020). The *Swift*/BAT data from a GUANO trigger are typically 200 seconds long with the trigger time centered in the middle, with exceptions if the telescope was maneuvering[3] (Tohuvavohu et al. 2020).

2. METHODS & TECHNIQUES

To determine fluence limits as well as make any possible detections I created an analysis pipeline in `Python` that runs from the terminal. The pipeline uses a catalog file that contains the *Swift* observation ID, RA, and Dec, the CHIME/FRB trigger time, and the CHIME/FRB ID for all the targets as an input. The pipeline has configurable parameters to govern the search criteria: energy bands, search window duration, number of time scales to use for the source detection, confidence level to use for the count limit, which *Swift* event files to use, and which spectrum models to use for the determination of fluence limits. HEASoft is the associated analysis software for *Swift*/BAT's, and was used extensively in the pipeline while XSPEC was used for fluence limits (Nasa High Energy Astrophysics Science Archive Research Center (Heasarc) 2014; Arnaud 1996).

The pipeline downloads the *Swift*/BAT data for the target if it is not already available locally, and performs its analysis resulting in measurements of the peak S/N and fluence limits for the target. The pipeline outputs a diagnostic plot for each target containing five or six figures: the target lightcurve, a zoomed in light curve around the search window, two histograms of the photon energy distribution over the same time windows as the light curves, a S/N vs peak time scale figure, and possibly a sky image if one was created by the pipeline. In addition the pipeline outputs a `json` file containing the peak S/N for each time scale and energy band, the fluence limits, and the count limit for each target.

2.1. *Source Detection*

For source detection we look for peaks in the S/N lightcurve over the search window duration centered at the CHIME/FRB trigger time. For this process the pipeline is using untargeted light curves. To do this I first have to construct the untargeted, mask weighted lightcurve for the target from the `.evt` file. The `.evt` file contains the time of every photon detection, the lightcurve is constructed by binning this data at a set timescale. I used untargeted lightcurves as the process for making targeted lightcurves for *Swift*/BAT reduces the effective area of the instrument and hence reduces the S/N (DeLaunay & Tohuvavohu 2022). Mask weighting takes into account hot pixels in a BAT detector. In addition, untargeted lightcurves have the advantage: sources that may be out of frame of the sky images may still be detectable as photons may come through the sides of the instrument.

To convert the lightcurve from photon counts into S/N, we subtract the mean and divide by the standard deviation of the lightcurve for a specified energy band. The peak in the S/N strongly depends on what timescale the resolution of the lightcurve is. I implemented a boxcar search method to search over the S/N lightcurve for peaks during the search window. I constructed a boxcar in length that corresponds to the search timescale[4], this is then convolved with the S/N lightcurve over the search window. The peak S/N per energy band per time scale is then the maximum of the convolution. This process is repeated for all energy bands combined, as well

[2] Or was conducting a specific observation.

[3] Not all the GUANO data corresponding to CHIME/FRBs will be usable. CHIME/FRBs could have been outside of the field of view of BAT, or the telescope could have been maneuvering to a new target.

[4] Normalized by the square-root of the length of the boxcar.

as each energy band specified, and for each timescale specified in the input parameters.

2.2. *Fluence Limits*

The key ingredients for fluence limits are the estimated Poisson count limit at the targets location, the Spectral Response File (RSP) file, and model spectrums. A fluence limit calculation is really weighting the count limit by the model spectrum. The RSP File contains the information about the effective area of the telescope for the position of interest as a function of the photon energy.

To determine fluence limits we must construct sky images of the target. This is due to the fact that *Swift*/BAT's RSP files which are needed to calculate fluence are generated for sky images, not lightcurves. Not all targets will be in the field of view of *Swift*/BAT, others may have issues in generating the RSP file. As such, not all targets will have fluence limits.

To generate the sky images I run the associated HEASoft commands for the data. This involved first making a detector plane image (DPI). In addition I make the corresponding noise image, and the RSP file. The image duration is matched with the search window centered on the CHIME/FRB trigger time. To determine the upper limit for the photon counts I used the `poisson_conf_interval` from astropy, using the kraft-burrows-nousek method (Astropy Collaboration et al. 2022; Kraft et al. 1991) With the event counts set as the counts in the sky image, and background counts as the counts from the noise image at the pixel value corresponding to the targets RA, DEC[5]. The fluence limits are then calculated by combining the count limit, RSP file, and model spectrums using `XSPEC`.

3. RESULTS

I searched for signals in a time window of ± 3 seconds around the CHIME/FRB trigger time and in energy bands ranging from 0-15, 15-25, 25-50, 50-100, 100-150, 200-250, and 250-350 keV, as well as in 13 logarithmically spaced timescales ranging from 0.01 to 6 seconds. The catalog used for the search consisted of 380 CHIME/FRB targets. Using the spectrum models listed in Table 1 fluence limits were determined in the $10-150$ keV band.

Of the 380 targets, the pipeline produced S/N outputs for 246 targets and fluence limits for 49 targets.

[5] For the purposes of this study, we only used the photon counts from a single pixel located at the CHIME localization. This is inaccurate as the CHIME localization is comparable to several pixels. However, soon CHIME baseband pipeline localizations will be available which are comparable to a single pixel.

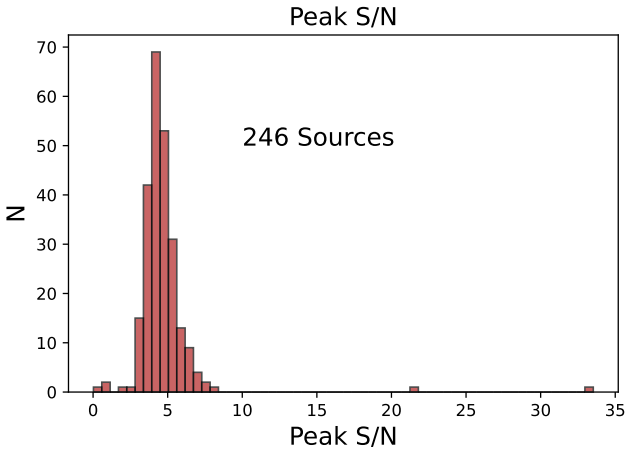

Figure 4: A histogram of the measured peak S/N of the targets searched with the analysis pipeline. There are two outliers from the analysis pipeline that had their diagnostic plots inspected by hand and determined to not be detections.

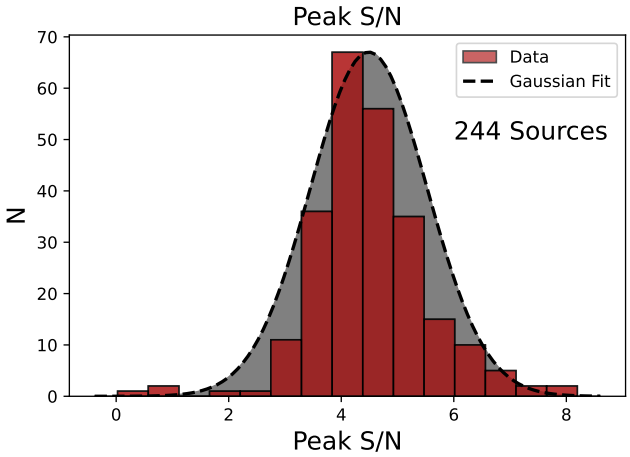

Figure 5: A histogram of the measured peak S/N of the targets with the outliers removed. On top of the histogram is a Gaussian with the same mean and standard deviation. The histogram is asymmetrical favoring higher S/N over lower S/N this is an artifact of measuring the peak S/N in the search window. The measured peak S/N closely resembles the Gaussian indicating that there are no significant events.

Results for the peak S/N are shown in Figure 4, and after removing two outliers in Figure 5. The fluence limits depend on the spectrum model which are listed in table 1, along with their respective fluence limits in the 10-150 keV band. Figure 6 compares the fluence limits, and distance estimations for the FRB targets.

4. DISCUSSION

Table 1: Model spectrum parameters from Scholz et al. (2017) with fluence limits (95% confidence) made by fitting to the peak count limit in `XSPEC`.

Model	N_H cm^{-2}	$\frac{KT}{\Gamma}$ keV/-	Fluence limit ($\times 10^{-7}$ ergs cm^{-2})
Blackbody	22	10	< 2
Blackbody	24	10	< 2
Cutoff PL	22	0.5	< 6
Cutoff PL	24	0.5	< 6
Soft PL	22	2	< 2
Soft PL	24	2	< 2

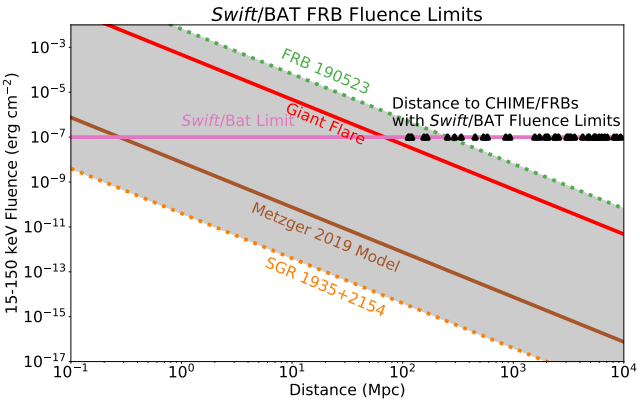

Figure 6: *Swift*/BAT fluence limits. The lines represent bursts of constant energy. The dashed lines bounding the grey region are the lower, and upper limits for FRB emission in γ-rays. The other lines are a lower energy limit for the (Wu et al. 2020), and a Magnetar Giant Flare for comparison. The magenta horizontal line represents the *Swift*/BAT fluence limits determined by the analysis pipeline. The black triangles represent the estimated distance to FRBs that had resulting fluence limits from the analysis pipeline.

No FRB was detected in γ-rays, the highest peak-S/N was 8 which is not significant enough for a detection as it cannot be discerned from noise.The diagnostic plots of the two outliers in the peak S/N were investigated by hand, and appear to be an instrumental noise artifact & some unknown artifact - not FRBs.

The analysis pipeline yielded S/N outputs for 246 out of the 380 CHIME/FRB targets in the catalog. That is a success rate of $\sim 65\%$ for the pipeline, which indicates that there are failure modes that need to be investigated and fixed. The failure modes for S/N estimation occur mostly during the boxcar search. A few targets fail in the lightcurve generation due to having the preferred event file. The pipeline produced fluence limits for 49 out of 246 targets which had S/N estimates. This is a reasonable number, as the *Swift*/BAT sky images looks at $\sim \frac{1}{8}$ of the sky. $\frac{244}{8} \approx 31$. The failures modes from the fluence limit are either failure to generate the RSP file, or the target is out of frame of the image.

Figure 6 indicates that the FRBs with fluence limits where obtained only for FRBs further away 10^2 Mpc. It appears possible that *Swift*/BAT may be able to make a detection for closer targets. This was a smaller catalog run then what is possible. The catalog used only contained 380 targets, while the true number of CHIME/FRB targets with *Swift*/BAT is greater than a thousand.

Future work consists of investigating and correcting if possible the failure modes, as well as running the analysis pipeline on a larger catalog.

5. CONCLUSION

I searched for γ-ray emission associated with Fast radio bursts (FRBs) using data from the *Swift*/BAT and a catalog of 380 CHIME/FRB targets. I applied a set of 6 spectrum models to search for signals in 7 energy bands ranging from 10-350 keV and 13 timescales from 0.01 to 6 seconds.

S/N estimates were determined for 244 sources with no FRBs being detected. Fluence limits for 49 CHIME/FRBs were determined at $\sim 10^{-7}$ergs cm^{-2} level in the 10-150 keV band (95% confidence). It remains possible that close FRBs may be able to be detected by *Swift*/BAT. The next steps in this research involve identifying and addressing the issues that led to failures, and analyzing a larger catalog of FRBs.

REFERENCES

Arnaud, K. A. 1996, in Astronomical Society of the Pacific Conference Series, Vol. 101, Astronomical Data Analysis Software and Systems V, ed. G. H. Jacoby & J. Barnes, 17

Astropy Collaboration, Price-Whelan, A. M., Lim, P. L., et al. 2022, ApJ, 935, 167, doi: 10.3847/1538-4357/ac7c74

Bandura, K., Addison, G. E., Amiri, M., et al. 2014, in Society of Photo-Optical Instrumentation Engineers (SPIE) Conference Series, Vol. 9145, Ground-based and Airborne Telescopes V, ed. L. M. Stepp, R. Gilmozzi, & H. J. Hall, 914522, doi: 10.1117/12.2054950

Barthelmy, S. D., et al. 2005, Space Sci. Rev., 120, 143, doi: 10.1007/s11214-005-5096-3

Bochenek, C. D., Ravi, V., Belov, K. V., et al. 2020, Nature, 587, 59, doi: 10.1038/s41586-020-2872-x

Chawla, P., Andersen, B. C., Bhardwaj, M., et al. 2020, ApJL, 896, L41, doi: 10.3847/2041-8213/ab96bf

CHIME Collaboration, Amiri, M., Bandura, K., et al. 2022, ApJS, 261, 29, doi: 10.3847/1538-4365/ac6fd9

CHIME/FRB Collaboration, Andersen, B. C., Bandura, K. M., et al. 2020, Nature, 587, 54, doi: 10.1038/s41586-020-2863-y

DeLaunay, J., & Tohuvavohu, A. 2022, ApJ, 941, 169, doi: 10.3847/1538-4357/ac9d38

Gajjar, V., Siemion, A. P. V., Price, D. C., et al. 2018, ApJ, 863, 2, doi: 10.3847/1538-4357/aad005

Gehrels, N., et al. 2004, Astrophys. J., 611, 1005, doi: 10.1086/422091

Kraft, R. P., Burrows, D. N., & Nousek, J. A. 1991, The Astrophysical Journal, 374, 344

Lorimer, D. R., Bailes, M., McLaughlin, M. A., Narkevic, D. J., & Crawford, F. 2007, Science, 318, 777, doi: 10.1126/science.1147532

Lu, W., Kumar, P., & Zhang, B. 2020, Monthly Notices of the Royal Astronomical Society, 498, 1397, doi: 10.1093/mnras/staa2450

Martone, R., Guidorzi, C., Margutti, R., et al. 2019, A&A, 631, A62, doi: 10.1051/0004-6361/201936284

Mereghetti, S., Savchenko, V., Ferrigno, C., et al. 2020, ApJL, 898, L29, doi: 10.3847/2041-8213/aba2cf

Nasa High Energy Astrophysics Science Archive Research Center (Heasarc). 2014, HEAsoft: Unified Release of FTOOLS and XANADU, Astrophysics Source Code Library, record ascl:1408.004. http://ascl.net/1408.004

Nicastro, L., Guidorzi, C., Palazzi, E., et al. 2021, Universe, 7, 76, doi: 10.3390/universe7030076

Petroff, E., Hessels, J. W. T., & Lorimer, D. R. 2022, A&A Rv, 30, 2, doi: 10.1007/s00159-022-00139-w

Petroff, E., Hessels, J. W. T., & Lorimer, D. R. 2022, Astron. Astrophys. Rev., 30, 2, doi: 10.1007/s00159-022-00139-w

Platts, E., Weltman, A., Walters, A., et al. 2019, PhR, 821, 1, doi: 10.1016/j.physrep.2019.06.003

Pleunis, Z., Michilli, D., Bassa, C. G., et al. 2021, ApJL, 911, L3, doi: 10.3847/2041-8213/abec72

Scholz, P., Bogdanov, S., Hessels, J. W. T., et al. 2017, ApJ, 846, 80, doi: 10.3847/1538-4357/aa8456

Scholz, P., Cook, A., Cruces, M., et al. 2020, ApJ, 901, 165, doi: 10.3847/1538-4357/abb1a8

Tohuvavohu, A., et al. 2020. https://arxiv.org/abs/2006.04550

Wu, Q., Zhang, G. Q., Wang, F. Y., & Dai, Z. G. 2020, ApJL, 900, L26, doi: 10.3847/2041-8213/abaef1